

**REGIONAL VARIATION OF RAYLEIGH-WAVE ATTENUATION
IN SOUTHERN ASIA PREDICTED FROM NEW MAPS OF LG CODA Q
AND ITS FREQUENCY DEPENDENCE AT 1 HZ**

Lianli Cong¹ and Brian J. Mitchell²

Yunnan University¹ and Saint Louis University²

Sponsored by Air Force Research Laboratory

Contract No. FA8718-04-C-0021

ABSTRACT

In order to ascertain whether or not seismic stations in low-Q regions, such as southern Eurasia, can detect small nuclear events and earthquakes, it is important to develop maps that show how Q varies regionally. In addition, in order to test the usefulness of seismic discriminants we must quantify the frequency dependence of Q and its variation from region to region. Toward those goals, we have (1) developed new continent-wide maps of Lg coda Q and its frequency dependence at 1 Hz (Q_0 and η respectively) with lower standard errors and improved resolution compared to earlier maps and (2) have used the new sets of Q_0 and η values to estimate how Rayleigh-wave attenuation varies through selected regions of Eurasia.

Our new maps of Q_0 and η cover virtually all of Eurasia but they concentrate especially on five regions where data coverage was absent or poor in earlier work. Those regions are southeastern China with new Q values for 165 new event-station pairs, India and the Himalaya with 269 new values, northeastern Siberia with 387 new values, Spain with 79 new values and southeast Asia with 43 new values. The maps provide new coverage throughout much of those five regions as well as much improved coverage in their peripheral portions. We have developed maps of standard errors for all determinations and maps of point spreading functions in selected regions in order to provide a measure of our ability to resolve features on the maps. Q_0 is relatively high, up to 700 or more, in most cratonic regions but low than expected in the Arabian craton (300 – 450), the Siberian trap portion of the Siberian Platform (~450) and the Deccan trap portion of the Indian Platform (450-650). It is generally low throughout the Tethysides orogenic belt but there too it displays substantial regional variations (150 – 400).

In our studies of Rayleigh-wave attenuation coefficients (γ_R) and their regional variation for various periods across southern Eurasia, we have assumed that the values of Q_0 and η obtained from Lg coda can be used to infer values of shear-wave Q (Q_μ) and its frequency dependence (ζ) with suitably chosen empirical scaling factors. We have tested this assumption for several crustal shear-wave Q models, one for the Arabian Peninsula, one for the Turkish/Iranian Plateaus and seven for China where determinations of Rayleigh-wave attenuation and Lg coda Q information are both available. We find that the relations $Q_\mu \propto Q_0$ at all depths and $\zeta = 0.8\eta$ for the depth range 0-40 km and $\zeta = 0.5\eta$ for depths greater than 40 km provide realistic estimates for γ_R in the period range 5 – 70 s. Throughout southern Asia γ_R at a period of 10s varies roughly between 0.3×10^{-3} and $1.7 \times 10^{-3} \text{ km}^{-1}$, at a period of 20 s varies between 0.2×10^{-3} and $0.9 \times 10^{-3} \text{ km}^{-1}$, and at 50s varies between about 0.06×10^{-3} and $0.30 \times 10^{-3} \text{ km}^{-1}$. Rayleigh-wave attenuation coefficients at 10s period are very sensitive to thick accumulations of sediments but that sensitivity is lost at 50s periods where variations in attenuation are due largely to regional variations in shear-wave Q in deeper crystalline rock.

OBJECTIVES

Seismic Q is an important parameter that affects how rapidly various seismic waves attenuate with distance as they travel through the Earth. Its value can vary both spatially and with frequency. The overall purpose of our research is to better understand details of those variations throughout southern Asia and how they might affect our ability to detect waves generated by small seismic events, to estimate magnitudes and yields of those events, and to determine if they are explosions or earthquakes. To improve understanding in those areas we have focused on two specific objectives. Our first objective has been to expand and improve previously published maps of regional variations of Lg coda Q across Eurasia with emphasis on regions where path coverage was too sparse to obtain reliable and high-resolution results. Our second objective has been to use those new maps of Lg coda Q and its frequency dependence at 1 Hz (Q_0 and η , respectively) to develop maps of Rayleigh-wave attenuation coefficients for various periods (10-50s) throughout southern Asia.

RESEARCH ACCOMPLISHED

Lg coda Q data and their processing

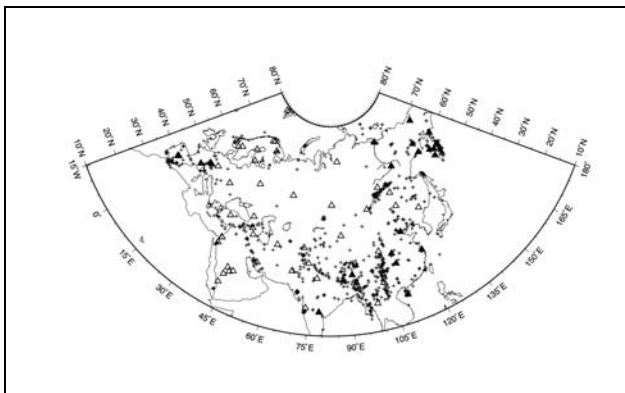


Figure 1. Earthquakes and stations used in this study. + signs denote earthquakes. Open circles denote stations used in Mitchell et al. (1997) and closed circles denote stations for new data.

Figure 1 presents a map of the earthquakes and recording stations used in this study. Data from 27 stations on the map are new to this study and provide recordings of Lg coda from 943 earthquake-station pairs. The new determinations, when combined with 440 from Mitchell et al., (1997) yield a total of 1383 determinations for both Q_0 and η . The new data provide new coverage for northeastern Siberia, where the largest gap previously existed, for Spain and for southeastern Asia. In addition, we achieved much improved coverage in northeastern China, southeastern China, and India.

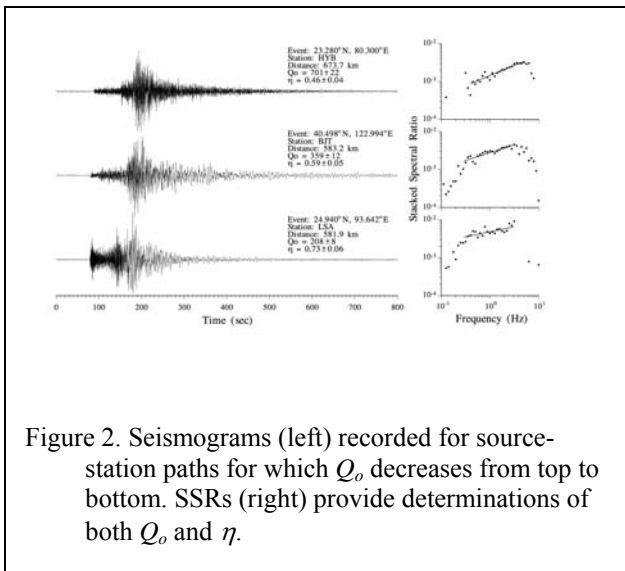


Figure 2. Seismograms (left) recorded for source-station paths for which Q_0 decreases from top to bottom. SSRs (right) provide determinations of both Q_0 and η .

Three examples of seismograms that include Lg and its coda for Eurasian paths appear in Figure 2. Measured values of Q_0 decrease from top bottom in the figure. The top trace is for a relatively high-Q (701) path to station HYB in India, the bottom trace is for a low-Q (208) path to station LSA in Tibet and the middle trace is from a path to station BJT in northern China where Q (359) is intermediate between the other two. The traces show a progression of decreasing predominant coda frequencies and decreasing amplitudes with decreasing Q value.

Stacked spectral ratio (SSR) plots (Xie and Nuttli, 1988) appear to the right of each trace. Portions of all three traces form an approximate straight line on a log-log plot that can be fit by least squares. The value and slope of the best-fitting line at 1 Hz yield, respectively, values for Q_0 and η from which we invert to obtain tomographic maps as described in the following section.

Mapping Q_0 and η variations – Method

A discussion of the inversion method for mapping Q_0 and

η appears, in detail, in Xie and Mitchell (1990), and more briefly, in Mitchell et al. (1997). The method assumes that the area occupied by the scattered energy of recorded Lg coda can be approximated by an ellipse with the source at one focus and the recording station at the other, as was shown theoretically by Malin (1978) to be the case for single scattering.

The process utilizes a back-projection algorithm for producing tomographic images of Q_0 and η over a broad region using a number (N_d) of Q_0 or η values determined from observed ground motion. Figure 3 shows the ellipses

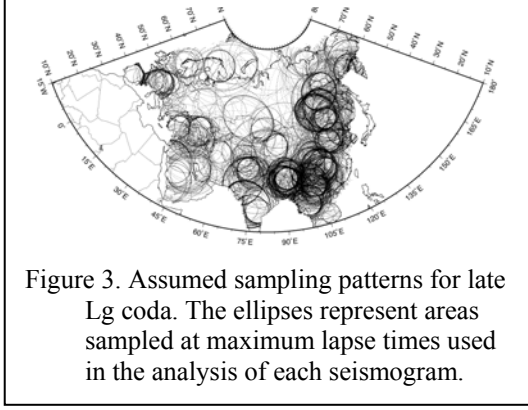


Figure 3. Assumed sampling patterns for late Lg coda. The ellipses represent areas sampled at maximum lapse times used in the analysis of each seismogram.

corresponding to all event-station pairs that we used in Eurasia. The inversion process assumes that each ellipse approximates the spatial coverage of scattered energy comprising late Lg coda. The areas of the ellipses vary with the lag time of the Lg coda components and will be larger for later times. The ellipses in the figure are plotted for maximum lag times used in the determination of Q_0 and η . It is best to have as much overlap of ellipses as possible to obtain redundancy that is beneficial in the inversion process.

We divided Eurasia into N_c cells with dimensions 3° by 3° , based upon theoretical resolution. over which Q_0 will have constant value. The Q_n value for each trace signifies the areal average of the cells covered by its corresponding ellipse. If the

area over which the ellipse for the n^{th} trace overlaps the m^{th} cell is s_{mn} then

$$\frac{1}{Q_n} = \frac{1}{S_n} \sum_{m=1}^{N_c} \frac{s_{mn}}{Q_m} + \mathcal{E}_n \quad n = 1, 2, \dots, N_d \quad (1)$$

where

$$S_n = \sum_{j=1}^{N_c} S_{jn} \quad (2)$$

and \mathcal{E} is the residual due to the errors in the measurement and modeling of Lg coda. Back-projection, or the Algebraic Reconstruction Technique [Gordon, 1974] has been applied in several tomographic mappings of seismic velocity (e.g. McMechan, 1983; Humphreys and Clayton, 1988) and is convenient for our purposes.

A tomographic map of the frequency dependence of Lg coda Q at 1 Hz is obtained using the Q_0 and η values for the N_d traces to estimate Lg coda Q at another frequency which we take to be 3 Hz. The 3-Hz values become Q_n in equation (1) and an inversion yields a map of Lg coda Q at 3 Hz. A map of the frequency dependence of Lg coda Q is then obtained using

$$\eta = \frac{1}{\ln 3} \ln \left[\frac{Q(f)_{3 \text{ Hz}}}{Q_0} \right] \quad (3)$$

For the back-projection process it is convenient to use the “point spreading function” (psf) suggested by Humphreys and Clayton [1988] as a measure of resolution. It is obtained constructing a model in which Q^{-1} is unity in a cell of interest and zero in all other cells. Average Q_0 is determined for all elliptical areas in Figure 3 for that model. An inversion of those synthetic data yields the psf pertaining to the region surrounding the selected cell. The area and falloff with distance from the central cell provides an estimate of resolution.

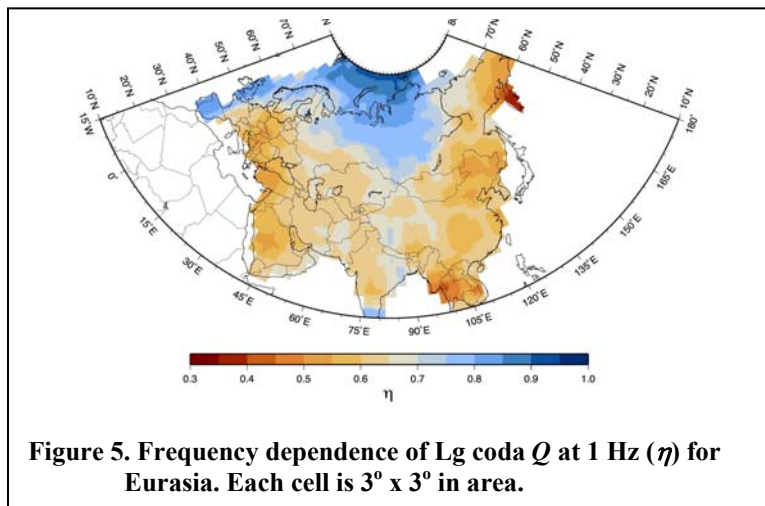
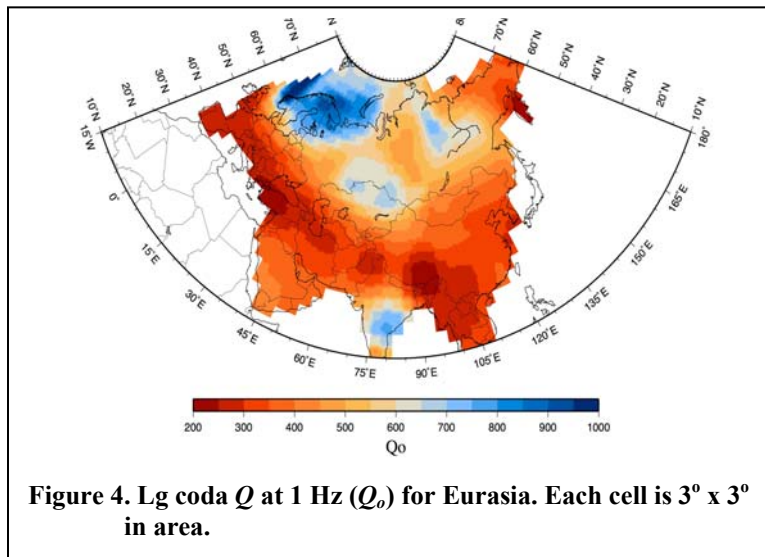
The effect that random noise included in Lg coda has on images of Q_0 and η can be tested empirically using the sample standard error in Q_n caused by randomness of the SSRs [Xie and Nuttli, 1988]. If the standard error of Q_n is denoted by δQ_n , $n = 1, 2, \dots, N_d$, and if we assume that δQ_n gives a good measure of the absolute value of real error preserved in the Q_n measurements, we can construct a number of noise series whose m^{th} member has an absolute value equal to δQ_n and a sign that is chosen randomly. The n^{th} term of the noise series is added to Q_n and the sums of the two series are then inverted to obtain a new Q_m image from which the original one is subtracted to yield an error

estimate of the Q_n values. Since the sign of δQ_n was chosen by a random binary generator, it is important to repeat the process several times and obtain an average error estimate.

New Q_o and η maps

Figures 4 and 5 are new continent-wide maps of Q_o and η for Eurasia. They differ from earlier continent-wide maps (Mitchell et al., 1997) by providing new coverage for northeastern Siberia, Spain, southern India and southeast Asia. In addition they provide much improved data coverage for several regions, including southeastern China, northeastern China, northern India and portions of northern Asia.

The broad-scale features of the new Q_o map are virtually the same as those of Mitchell et al. (1997) for regions where there is common coverage. These include low values (150 – 400) throughout, and extending slightly north of,



the Tethysides orogenic belt, the active region resulting from the collision of the Afro/Arabian and Indian plates with Europe and Asia, and significantly higher values (as high as 950 or more) throughout most of the stable northern portions of Eurasia. There are, however, some unexpected results including relatively low values in central Siberia, and the Arabian Peninsula that were reported by Mitchell et al. (1997). The present study differs from

Mitchell et al. (1997) by finding lower than expected values in the British Isles and by showing four regions of very low Q that appear to be associated with concentrated seismic activity in western Turkey, Pakistan and northern India, southern China and Kamchatka. These apparently anomalous values are consistent with our previous suggestion that seismic Q values in the crust of continents in any region are proportional to the time that has elapsed since the most recent tectonic or orogenic activity there (Mitchell and Cong, 1998).

Q_0 is relatively high, 700 - 900 or more, in most cratonic regions in northern Eurasia but is surprisingly low in the Arabian craton (300 – 450), the Siberian trap portion of the Siberian Platform (~450) and the Deccan trap portion of the Indian Platform (450-650). It is generally low throughout the tectonically active Tethysides orogenic belt but there too it displays substantial regional variations (150 – 400).

Figure 5 presents the distribution of η , the frequency dependence of Lg coda Q at 1 Hz. Since its determination requires the differencing of Q_0 values at two frequencies, the uncertainties in mapped values η are much higher than for Q_0 . η values are generally higher (0.7 – 0.9) in regions where Q_0 is high (e.g., northern Eurasia and southern

India) and are low (e.g. most of southern and eastern Eurasia) where Q_0 is low. The opposite relation occurs in Spain and the British Isles, where Q_0 is low and η is high. It is possible that systematic errors in the differencing process for determining η are high in that region.

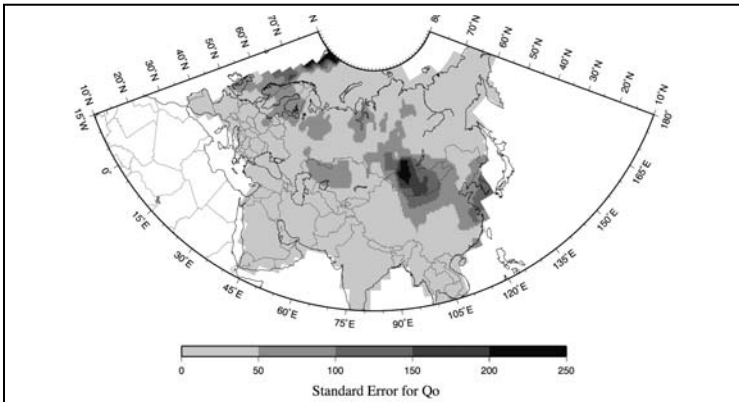


Figure 6. Standard errors for Q_0 .

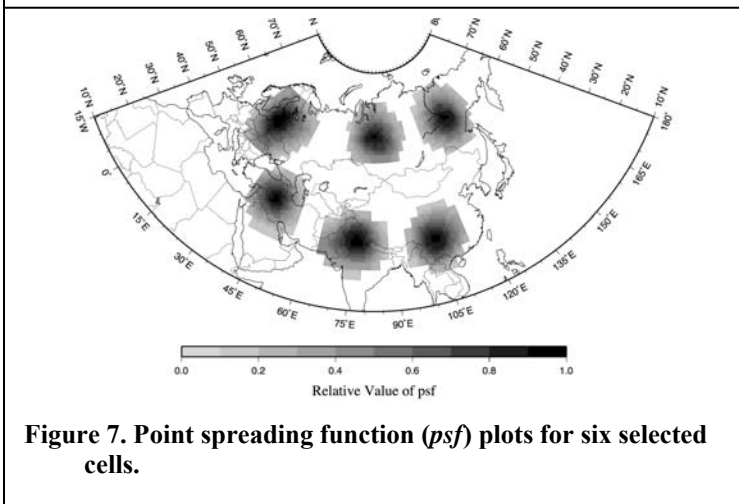


Figure 7. Point spreading function (psf) plots for six selected cells.

Figures 6 is a map of standard error values for Q_0 . The errors range between 0 and 50 throughout most of Eurasia but lie between 50 and 100 in a few places, and is quite high in regions to the southwest of Lake Baikal and in the northwestern corner of the map. The high standard errors near Lake Baikal coincide with a region that stood out as being laterally anomalous in a study of shear-wave Q variation (Jemberie and Mitchell, 2004). The pattern of η standard error variation is generally similar to that of Q_0 , being between 0.0 and 0.1 throughout most of the continent and between 0.1 and 0.2 in most other places. It is again higher to the southwest of Lake Baikal and in the northwestern-most corner of the map.

The psf patterns for six selected cells appear in Figure 7. They indicate that our ability to resolve features across Eurasia is about the same everywhere. Assigning numbers to this resolvability is somewhat subjective, depending upon what we

choose as a fraction of the maximum value that is assumed to denote resolvability but appears to indicate that we can resolve features between about 600 and 900 km in most regions. This marks a significant improvement over resolution in Mitchell et al.(1997) where the psf 's in some regions, especially where coverage was much poorer, was greater than 1500 km or more.

We used the values of Q_0 and η for Lg coda at 1 Hz to estimate Rayleigh-wave attenuation at periods of 10, 20 and 50 s for all of southern Asia. We assumed that the values of Q_0 in Figure 4 represent average values

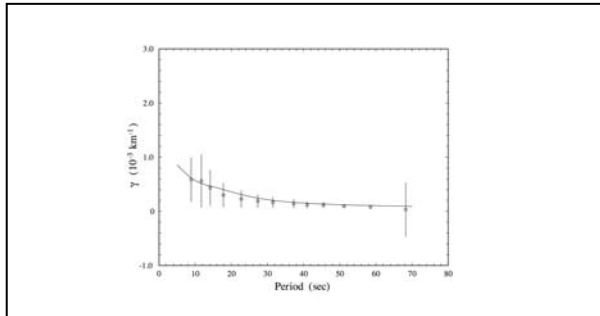


Figure 8. Rayleigh-wave attenuation coefficients calculated for a shear-wave Q model of the Arabian Peninsula in which $Q_\mu = Q_0$, $\zeta = 0.8\eta$ for depths less than 40 km and $\zeta = 0.5\eta$ for depths greater than 40 km (solid line). These are compared with Rayleigh-wave attenuation coefficients obtained from two-station measurements in the same region.

of shear-wave Q (Q_μ) for the crust everywhere in that region. We then developed an empirical relation between η values in Figure 5 and the frequency dependence (ζ) of shear-wave Q (Q_μ) in order to compute Rayleigh-wave attenuation coefficients produced by inferred Q_μ models of the crust. To do that we used observed Rayleigh-wave attenuation coefficients for regions where they are available to Rayleigh-wave attenuation coefficients values that are theoretically predicted by the Q_0 and η values for the same regions in Figures 4 and 5. Both types of information are available for the Arabian Peninsula and Turkish/Iranian Plateaus (Cong and Mitchell, 1998), as well as seven regions of China (Jemberie and Mitchell, 2004). One example comparison of observed and computed attenuation coefficients appears in Figure 8 for the Iran/Turkey Plateaus. We found that using the relations $\zeta = 0.8\eta$ for the depth range 0-40 km and $\zeta = 0.5\eta$ for depths greater than 40 km provided realistic

estimates for γ_R over the period range 10-70 s for most regions of southern Asia.

Maps of Rayleigh-wave attenuation estimates for southern Asia

Figures 9, 10, and 11 present predicted Rayleigh-wave attenuation coefficient values for periods of 10, 20 and 50 s, respectively. At a period of 10 s Rayleigh-wave attenuation coefficients vary between about 0.3×10^{-3} and $1.7 \times 10^{-3} \text{ km}^{-1}$, while at 20 s they vary between about 0.2×10^{-3} and $0.9 \times 10^{-3} \text{ km}^{-1}$, and at 50 s they vary between about 0.06×10^{-3} and $0.30 \times 10^{-3} \text{ km}^{-1}$. The patterns of Rayleigh-wave attenuation are generally similar to the patterns of Q_0 variation in Figure 4, but important differences occur, mainly because of variations in the frequency dependence of shear-wave Q used to calculate the Rayleigh-wave attenuation maps.

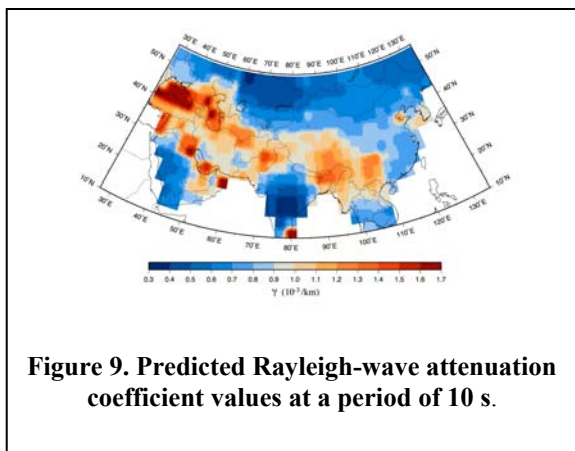


Figure 9. Predicted Rayleigh-wave attenuation coefficient values at a period of 10 s.

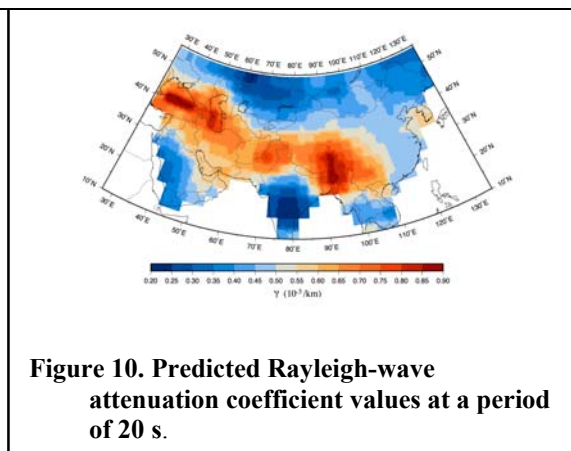
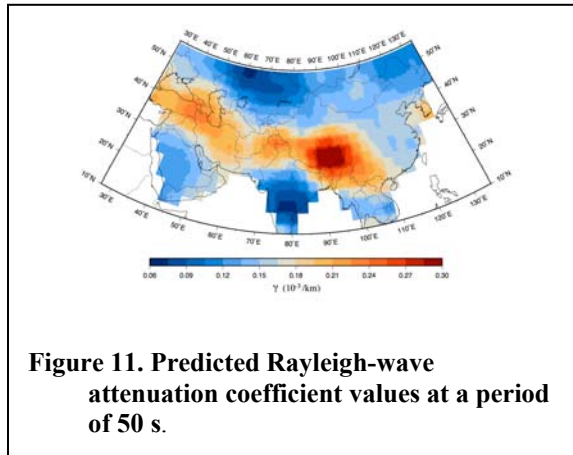


Figure 10. Predicted Rayleigh-wave attenuation coefficient values at a period of 20 s.

Rayleigh-wave attenuation is especially sensitive to accumulations of thick sediments in regions such as the Black Sea and Persian Gulf. At longer and longer periods there is less and less correlation with sediments but greater sensitivity to anelasticity in the crystalline crust. The highest attenuation at 50 s period occurs as a striking large circular region in the southeastern Tibetan Plateau, a region previously found to be highly attenuative for Lg coda (Mitchell et al., 1997) and extremely attenuative for direct Lg (Xie, 2002).



CONCLUSIONS AND RECOMMENDATIONS

New maps of Lg coda Q and its frequency dependence at 1 Hz (Q_0 and η , respectively) for virtually all of Eurasia show order of magnitude variations that certainly need to be accounted for in determinations of yield and in implementing many discrimination methods. The variations clearly reflect past tectonic activity, with lowest values being in regions of present or recent tectonic and/or orogenic activity. The maps of Q_0 and η values allow the construction of Rayleigh-wave attenuation coefficient maps at various frequencies, assuming that the value of the frequency-dependence parameter remains constant over a wide frequency range. These new maps show that thick accumulations of sediment have a large effect on 10 s Rayleigh-wave amplitudes, but little effect on the amplitudes at 50s.

Studies of the frequency dependence of Q are still rudimentary and much work in this area remains to be done. The usefulness of our maps of Rayleigh-wave attenuation depend strongly on how well the frequency dependence of Lg coda Q near 1 Hz frequency has been determined and on our assumption that its value does not change between 1 Hz and surface-wave frequencies. We recommend that systematic studies of that parameter be conducted from frequencies near 10 Hz down to intermediate-range surface-wave frequencies.

ACKNOWLEDGMENTS

We thank Jack Xie for making his codes for the SSR method of processing and for tomographic mapping of Q_0 and η available to us. The maps in this paper were prepared using GMT version 3.0 developed by Paul Wessel and H.F. Smith.

REFERENCES

- Cong, L. and B. J. Mitchell (1998), Seismic velocity and Q structure of the Middle Eastern crust and upper mantle from surface-wave dispersion and attenuation, *Pure Appl. Geophys.* 153: 503-538.
- Gordon, R. (1974), A tutorial on ART, *IEEE Trans. Nucl. Sci.* NS-21: 78-93.
- Humphreys, E. and R. W. Clayton (1988), Adaptation of back projection tomography to seismic travel time problems, *J. Geophys. Res.* 93: 1073-1086.
- Jemberie, A. L. and B. J. Mitchell (2004), Shear-wave Q structure and its lateral variation in the crust of China and surrounding regions, *Geophys. J. Int.* 157: 363-380.
- Malin, P. E. (1978), A first-order scattering solution for modeling lunar and terrestrial seismic coda, *Ph.D. dissertation*, Princeton Univ., Princeton, NJ.
- McMechan, G. A. (1983), Seismography in boreholes, *Geophys. J.R. Astr. Soc.* 74: 601-612.
- Mitchell, B.J., Y. Pan, J. Xie, and L. Cong (1997), Lg coda variation across Eurasia and its relation to crustal evolution, *J. Geophys. Res.* 102: 22767-22779.

27th Seismic Research Review: Ground-Based Nuclear Explosion Monitoring Technologies

Mitchell, B.J., and L. Cong (1998), Lg coda Q and its relation to the structure and evolution of continents: A global perspective, *Pure Appl. Geophys.* 153: 655-663.

Xie, J. (2002), Lg Q in the eastern Tibetan Plateau, *Bull. Seism. Soc. Am.* 92: 871-876.

Xie, J., and O.W. Nuttli (1998), Interpretation of high-frequency coda at large distances: Stochastic modeling and method of inversion, *Geophy. J.* 95: 579-595.

Xie, J., and B.J. Mitchell (1990), A back-projection method for imaging large-scale lateral variations of Lg coda Q with application to continental Africa, *Geophys. J. Int.* 100: 161-181.